Aerial Grasping and the Velocity Sufficiency Region

Tony G. Chen*[1], Kenneth A. W. Hoffmann*[1], Jun En Low[2], Keiko Nagami[2], David Lentink[3], Mark R. Cutkosky[1]

***Abstract*—A largely untapped potential for aerial robots is to capture airborne targets in flight. We present an approach in which a simple dynamic model of a quadrotor/target interaction leads to the design of a gripper and associated velocity sufficiency region with a high probability of capture. A model of the interaction dynamics maps the gripper force sufficiency region to an envelope of relative velocities for which capture should be possible without exceeding the capabilities of the quadrotor controller. The approach motivates a gripper design that emphasizes compliance and is passively triggered for a fast response. The resulting gripper is lightweight (23 g) and closes within 12 ms. With this gripper, we demonstrate in-flight experiments that a 550 g drone can capture an 85 g target at various relative velocities between 1 m/s and 2.7 m/s.**

***Index Terms*—Grasping, Mechanism Design, Aerial Systems: Application.**

I. Introduction

AERIAL robots such as quadrotors provide unparalleled versatility as a platform for tasks such as surveying, photography, and inspection [1]. While these applications have matured, quadrotors' interaction with their physical environments is still limited. As a result, many environmental interactions that require precision are slow, risky, and limited in force. In the case of aerial grasping, the grasping drone must be capable of compensating for a significant linear and angular disturbance. Establishing the flight conditions that maximize the likelihood of a successful aerial grasp is essential to informing drone control strategies. Practical use cases for aerial grasping drones include airports, where rogue drones can affect airspace operations.

In this paper, we present design considerations for a gripper and controller that can grasp airborne objects. We develop a *sufficiency region*, adapted in part from a sufficiency region previously developed while studying birds and drones perching on stationary branches [2]. The sufficiency region defines the envelope of velocities for which a successful grasp is expected – as a function of gripper design and drone controller parameters. The sufficiency region leads to the design of a gripper with a very low weight that uses stored internal energy for grasping when triggered by contact. However, unlike previous work focused on perching, this proposed work focuses on aerial grasping, where momentum is mostly conserved.

Fig. 1. Composite photo of the grasping sequence. Top: grasping drone moving at $2\,\mathrm{m\,s^{-1}}$ catching a moving target drone at $0.5\,\mathrm{m\,s^{-1}}$. Bottom: grasping drone at $2.7\,\mathrm{m\,s^{-1}}$ catching a hovering target.

In the following sections, we first review key areas of prior work related to this investigation. We then present a simplified model of the dynamics of a drone and gripper contacting an airborne target to identify gripper design objectives. We present the detailed design of a gripper that meets the objectives. Next, we characterize its performance in controlled tests. The result is an empirical force sufficiency region that describes the necessary contact forces for a successful grip. Using the drone dynamics, the force sufficiency region is mapped to a velocity sufficiency region for a drone with a standard controller. Finally, we demonstrate the capability of the drone and gripper in airborne grasping experiments and discuss future extensions.

Manuscript received: Feb. 24, 2022; Revised May 20, 2022; Accepted June 16, 2022. This paper was recommended for publication by Editor Hong Liu upon evaluation of the Associate Editor and Reviewers' comments. This research was supported by AFOSR DESI award FA9550-18-1-0525; we thank B.L. Lee, F.A. Leve, and J.L. Cambier for leading the program. T. G. Chen and K. A. W. Hoffmann are supported by NSF GRFP. K. A. W. Hoffmann is also supported by the Stanford Graduate Fellowship.

∗These authors contributed to this work equally.

[1]T.G. Chen, K. A. W. Hoffmann, and M. Cutkosky are with the Dept. of Mech. Engineering, Stanford University, Stanford, CA 94305. {agchen, khffmnn, dlentink, cutkosky} @stanford.edu.

[2]Jun En Low and Keiko Nagami are with the Dept. of Aeronautics and Astronautics, Stanford University, Stanford, CA 94305. {jelow, knagami} @stanford.edu.

[3]D. Lentink is with the Faculty of Science and Engineering, University of Groningen, Groningen, The Netherlands.

Digital Object Identifier (DOI): .

A. Related Work

Although the acquisition of flying targets appears to be new, the work reported here builds upon prior work on perching and grasping terrestrial targets.

Grasping drones can use various mechanisms to catch and secure their targets. Each of these methods has advantages and disadvantages, for example, trading grasp security or precision for speed of actuation. Diverse examples include grasping objects with magnets [3] [4], suction [5], arrays of spines [6], and lightweight nets [7]. To provide rapid actuation, teams have used stored elastic energy, although the associated gripper mechanisms may increase weight [2, 8, 9].

There are three distinct stages to aerial grasping: pursuing the target before collision, acquisition, and successfully flying with it after capture. Control of aerial grasping increases the likelihood of successfully catching the target. Several related papers have addressed the design, simulation, and control of aerial grasping robots. These works consider the tracking and pursuit of grasping targets in experiments and simulations [10]–[13]. Drones typically use cameras or motion capture systems to detect their targets. For tracking and pursuit, these cameras detect simple shapes such as cylinders and spheres. The position of the target is fed into a trajectory generator and visual servoing is used to pursue and catch the target [14]. The approach in [15] synthesizes a detection and pursuit scheme for grasping and piercing a balloon attached to another quadrotor in flight and demonstrates a level of autonomy for the aerial grasping problem. In the presented work, we focus on the mechanics of target acquisition.

The capture of an airborne target presents a challenge for a drone controller, which must compensate both for the contact forces during acquisition and the change in inertia and center of mass [10, 13, 16]. When capturing stationary or terrestrial targets, many aerial grasping robots slow down and grasp gradually to minimize the disturbance [12]. However, a moving target may instead try to change its trajectory so that a slow acquisition is not possible. Some groups have also demonstrated grasping at high speed for grounded targets [9, 13]. The acquisition in this case can benefit from the added friction and stability of ground support for the target. On the other hand, a solution that works for unrestrained airborne targets, as we consider in this paper, is likely to work for stationary targets as well.

Drone perching has also been addressed by several groups (e.g. [2, 17]–[21]) and shares similar concerns as the presented work. One difference is that the absolute velocity of a perching drone is zero at the end of a perching sequence, so all kinetic energy must be stored and/or dissipated. In contrast, for grasping an aerial target, some kinetic energy remains after capture. This leads to a design philosophy that favors a light triggering force. Still another area of related work is the acquisition of thrown targets with a stationary arm and gripper (e.g. [22, 23]). However, in most such work it is assumed that the arm is fixed to a stationary base allowing high torques at the joints, correspondingly fast motions, and relatively large contact forces during acquisition.

B. Contribution

A primary contribution of this paper is a modeling approach that maps the problem of acquiring an airborne target to a velocity sufficiency region, for which a given gripper and drone should be able to acquire and secure a target of a given mass and inertia. It outlines the steps necessary to translate a traditional force space characterization of a robotic gripper to this velocity sufficiency region, which provides an array of vectors of possible relative velocity at the point of collision. These vectors can be used as the input to standard off-the-shelf drone controllers and hardware.

To demonstrate this approach, this paper presents a new, fast, and lightweight gripper with a built-in suspension system that can grasp another airborne drone in-flight at up to $2.7\,\mathrm{m\,s^{-1}}$ relative velocity.

II. Approach

A. Simplified quadrotor dynamics with collision

Traditional gripper testing in robotics is done in force space, e.g. with six-axis force-torque sensors. However, drones are commonly controlled using velocity commands, which are fed into a cascaded controller to adjust the speeds of the motors that power the propellers [10, 24].

For a gripper to be integrated and used by a drone platform, characterizing gripper sufficiency in velocity space is a beneficial choice. This provides the inputs for a drone controller with a focus on the gripping. Most drone controllers are in position, velocity, and attitude space, although there are some specific cases where force control is used in tool operation [25], and controlling contact [26, 27].

To explore the mapping from interaction forces to velocities in more detail, we can consider a drone as depicted in Fig. 2.

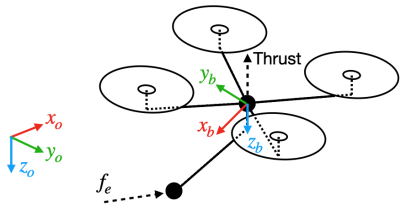

Fig. 2. Quadrotor schematic.

A common approach to write the dynamics is [25]:

$$m\ddot{\boldsymbol{x}} = \boldsymbol{R}\boldsymbol{f_u} + mg\boldsymbol{e_3} + \boldsymbol{f_e} \tag{1}$$

$$\boldsymbol{I}\dot{\boldsymbol{\omega}} = \boldsymbol{I}\boldsymbol{\omega} \times \boldsymbol{\omega} + \boldsymbol{\tau_u} + \boldsymbol{\tau_c} \tag{2}$$

where $\boldsymbol{x}$ is the drone's center-of-mass position in the inertial frame, m is the mass, $\boldsymbol{f_u}$ is the thrust vector, $\boldsymbol{f_e}$ is the vector of the interaction force, g is the gravitational constant, and $\boldsymbol{e_3} = [0, 0, 1]^T$ is a basis vector specifying the direction, $\boldsymbol{I}$ is the inertia matrix, $\boldsymbol{\omega}$ is the angular velocity vector, $\boldsymbol{\tau_u}$ is the torque input for the drone, $\boldsymbol{\tau_c}$ is the external torque applied to the drone by the interaction and $\boldsymbol{R}$ is a transformation matrix between the world frame $\{\boldsymbol{O}\}$ and the body frame $\{\boldsymbol{B}\}$ of the drone.

Assuming that the gripper is rigidly attached to the drone, $\boldsymbol{\tau_c}$ and $\boldsymbol{f_e}$ are related through the distance between the end of the gripper to the center-of-mass of the drone, $\boldsymbol{d}$,

$$\boldsymbol{\tau_c} = \boldsymbol{d} \times \boldsymbol{R^T f_e} \tag{3}$$

For the drone to remain stable after the intentional collision, it must recover from the external wrench applied by the collision. Note that $\boldsymbol{f_u}$ and $\boldsymbol{\tau_u}$ are generated by a feedback policy on the drone's state. As a simple best-case approximation we can assume they are related to the maximum rotor speeds:

$$\begin{bmatrix} \boldsymbol{f_u} \\ \boldsymbol{\tau_u} \end{bmatrix} = \begin{bmatrix} -k_f & -k_f & -k_f & -k_f \\ -k_f L_y & k_f L_y & k_f L_y & -k_f L_y \\ k_f L_x & -k_f L_x & k_f L_x & -k_f L_x \\ k_M & k_M & -k_M & -k_M \end{bmatrix} \begin{bmatrix} \omega_1^2 \\ \omega_2^2 \\ \omega_3^2 \\ \omega_4^2 \end{bmatrix} \tag{4}$$

where ω_i is the angular speed of each rotor on the drone, k_f, k_M are respectively the motor thrust constant and motor torque constant, and L_x, L_y are the distance between the center of the motor and the CoM of the drone, in the x_b and y_b frame respectively. Performing this calculation with the maximum angular speed of each of the rotors on the drone results in a maximum $\boldsymbol{f_u}, \boldsymbol{\tau_u}$, which can be used in eq. (1, 2) to find the maximum external wrench that can be applied during a collision consistent with controller limitations.

The change in momentum of the drone caused by this interaction, approximating the controlled collision as an impulse, becomes

$$\Delta(M\boldsymbol{v}) = \int_{t_o}^{t_g} \boldsymbol{f_e} dt \tag{5}$$

$$\Delta(I\boldsymbol{\omega}) = \int_{t_o}^{t_g} \boldsymbol{d} \times \boldsymbol{R^T f_e} dt \tag{6}$$

where $\Delta(M\boldsymbol{v})$ and $\Delta(I\boldsymbol{\omega})$ are the change in linear momentum and angular momentum, respectively. The period between initial contact and when the difference in velocity between the drone and its target is insignificant is defined by $(t_g - t_o)$.

B. Defining the velocity sufficiency region

Traditionally, robotic grippers are evaluated in terms of their acquisition region and their ability to hold objects securely [28, 29]. A limit surface in wrench space can represent the maximum forces and moments. Unlike a rigidly mounted arm, a drone typically cannot apply or resist large forces and moments that arise from the collision event. Thus the limit surface for aerial grasping needs to be augmented with the dynamic limitations of the drone. The combined sufficiency region can be translated into the velocity space with the relationship between relative velocity and collision force. The resulting velocity sufficiency region can be used in conjunction with a flight controller. This process is highlighted in Fig. 3.

III. Gripper Design

The implications of eq. (5,6) are that one should reduce $|\boldsymbol{f_e}|$ as much as practical while also keeping the interval $(t_g - t_o)$ brief. Considering the gripper and its suspension, the former goal can be accomplished by introducing compliance and friction to dissipate energy while there is still relative motion between the gripper and its target. The latter goal motivates a fast-acting gripper. A fast-acting gripper also reduces the chance that the target will escape or bounce out of the grasp before the gripper closes.

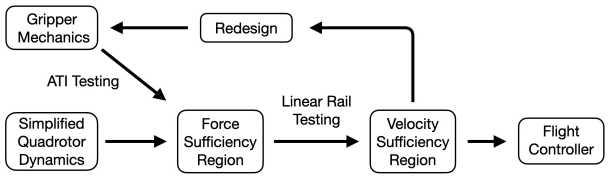

Fig. 3. Road-map to employ the velocity sufficiency region.

At the same time, general objectives for the gripper system include: (i) the overall weight and inertia should be minimized, (ii) the maximum allowable difference in initial relative velocity between the gripper and target should be as large as possible and (iii) the combination of gripper and target should impose payload torques as small as possible after target acquisition is complete.

A. Design Approach

1) Passive Grasping: Given the aforementioned objectives, we developed a passively-triggered gripper mounted on a compliant suspension, as illustrated in Fig. 4. The use of a passive triggering mechanism eliminates the need for sensors to detect and respond to contact with the target and allows the gripper to use stored potential energy for fast closure. It also avoids the weight and complexity of a system with sensors, actuators , and electronics. We observe that for similar reasons, passively triggered grippers have been used in other work for perching and grasping terrestrial targets (e.g. [2, 9, 30]).

In the following paragraphs, we present the elements of the gripper and suspension. The gripper and suspension weigh $22.7\,\mathrm{g}$, roughly 4.2% of the weight of the drone.

2) Trigger Mechanism: The trigger system consists of a tendon tied to the linear compliance mechanism that rotates a trigger upon movement. This trigger nominally holds rubber bands tight, storing potential energy, and releases this potential energy upon triggering. The stored potential energy is used to close the underactuated gripper, through the use of another tendon. The low force needed to activate this trigger system is proportional to the force provided by the loaded rubber bands and the stiffness from linear compliance. The mechanism requires human interaction to reset between trials.

The passive triggering mechanism is detailed in Fig. 4(B), where two rubber bands with a spring constant of $106\,\mathrm{N\,m^{-1}}$ are stretched between the block (in yellow) and fixture, to provide a total of $4.8\,\mathrm{N}$ of force. A trigger initially stops the block from sliding forward, thus storing the potential energy inside of the gripper. This trigger is tied to the trigger tendon, shown in Fig. 4(F) in red. It has a fixed point at the front of the gripper and loops around the movable section of the linear

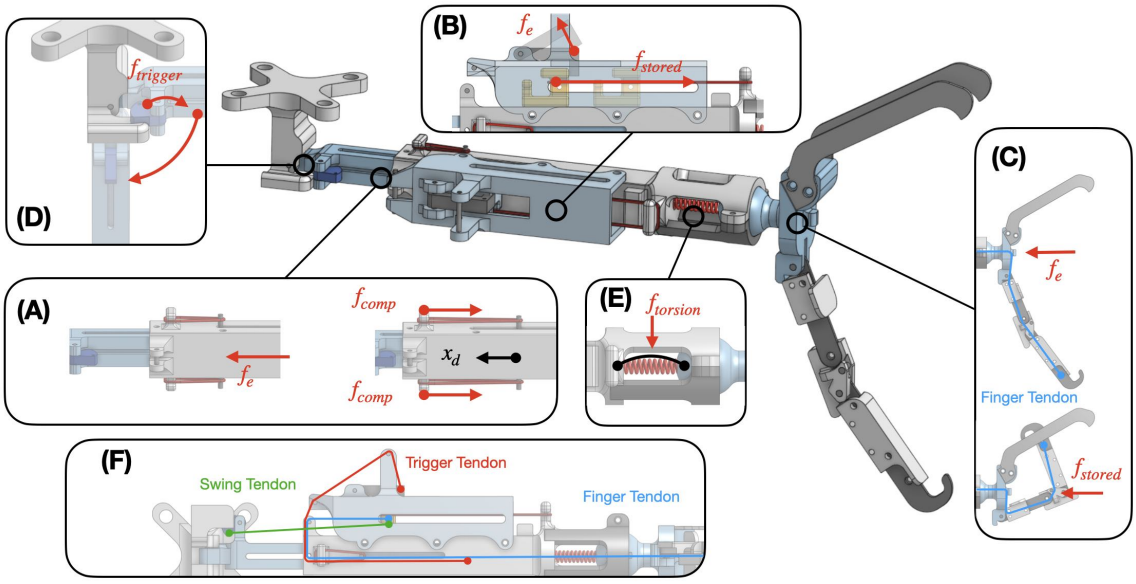

Fig. 4. Detailed gripper mechanism. (A) shows the main linear compliance mechanism consists of two segments of the main gripper body and rubber bands. (B) shows the gripper trigger mechanism where the impact causes the trigger tendon to shorten, pulling the trigger piece to release the stored energy. (C) shows the underactuated finger where upon impact force releasing the trigger, the stored energy is used to close the gripper and hold the position. (D) shows the optional swinging mechanism that enables the gripper to swing down after impact. (E) shows the ball joint connecting the under-actuated finger to the main body of the gripper, with a compression spring embedded in the structure to provide the rotational compliance, and (F) illustrates the three tendons used in the gripper mechanism and its routing.

compliance mechanism. As soon as the impact occurs, the linear compliance mechanism starts to compress, causing the trigger tendon to pull the trigger upward, releasing the stored potential energy. The finger tendon (shown in Fig. 4(C)(F) in blue) is tied to the block. The motion of the block traveling forward due to the stored energy closes the under-actuated finger for a fast grasp. The gripper can close around an object within $12\,\mathrm{ms}$ of first contact. The required triggering force is described by

$$f_f = C\mu f_{stored} \tag{7}$$

where μ is the coefficient of friction between the trigger piece and the block, f_{stored} is the total spring force applied to the block, and C is a constant to account for the inefficiency in force transferred through the tendon routing.

3) Gripper Compliance: Gripper mechanism compliance is one effective way of reducing the loading on the drone during the collision. Additionally, including compliance increases the collision duration. Part of the kinetic energy will be absorbed into the system based on the spring stiffness of the compliance mechanism k_{comp}, and the total travel distance x_{comp}. However, there is also a trade-off because compliance affects the force needed to trigger the gripper:

$$f_{trig} \geq k_{comp} x_{comp} + f_f \tag{8}$$

where f_{trig} is the triggering force needed for the mechanism to start grasping, and f_f is the friction force inside of the actual trigger mechanism. With increased stiffness, k_{comp}, more force can be absorbed upon collision, which helps to reduce $|\boldsymbol{f_e}|$. However, this is accomplished at the cost of increasing the minimal impact force needed to trigger the grasping mechanism, increasing the risk of a collision without attempts to grasp. Additional energy can be dissipated in any viscoelastic or frictional connections inside of the gripper mechanism.

4) Linear Compliance Suspension: The body of the gripper suspension is made up of two square tubular structures, shown in Fig. 4(A). The front tube can slide along the back tube with a limit set by an internal dowel pin. Two rubber bands with a spring constant of approximately $30\,\mathrm{N\,m^{-1}}$ are tied to the two sides of the structure (in red) to provide linear compliance in the longitudinal direction. Upon impact with an object, this linear compliance serves two functions: (i) to absorb kinetic energy to lessen the magnitude of the impact force, and (ii) to increase the time of contact between the gripper and the object, so the gripper has more time to fully close before the target object bounces off. However, as noted earlier, an implication of eq. (5,6), is that increasing the time is only desirable if doing so also decreases $|\boldsymbol{f_e}|$.

5) Under-actuated Finger: One common solution to achieve enveloping or partially enveloping grasps on convex objects is through the use of an under-actuated hand [31]. The single under-actuated claw of the gripper, shown in Fig. 4(C), is designed to be able to close around a 20mm rod, or similarly shaped objects. It is made up of two fixed, carbon-fiber fingers on the top and one under-actuated, two-segment finger at the bottom. The key to increasing the probability of a successful grasp is to ensure that the proximal joint closes first and the distal joint closes second, securing an enveloping grasp around the target object.

6) Ball Joint: The claw is connected to the rest of the gripper through a self-centering ball-joint Fig. 4(E). This is achieved using a compression spring between the main structure of the gripper and the ball joint where the claw is connected. Because of the torsional spring stiffness provided

by this compression spring, it allows for the gripper to be misaligned with the target at the point of impact while always staying nominally centered. Additionally, it helps to reduce moments transmitted to the quadrotor from contacts within the gripper, by reducing the moment when an impact is not directly at the center of the gripper.

7) Swinging Mechanism: As observed in nature, where the falcon swings its leg backward upon catching the prey [32], the gripper presented also has the capability of passively swinging downwards after a grasping attempt. A similar approach was taken in [13], albeit actively with a servo, to reduce the relative velocity. The swing tendon (Fig. 4(F) in green) is tied to the block in the triggering mechanism. When the trigger mechanism is activated due to an impact, the block is pulled forward by the rubber band, pulling this swing tendon forward as well. This forward motion rotates a disk that holds the gripper horizontal (Fig. 4(A)), releasing the gripper from its rotational position, enabling the downward swinging motion.

This mechanism serves two functions. The first is to reduce the relative velocity between the grasping drone and the target at the point of the impact. The second is to move the center of gravity of the captured target to a more favorable position, which is from the front of the drone to directly underneath the drone. This increases the stability of the grasping drone after a successful capture. This feature was not used for the flight tests in Section.V(D), as it added some undesirable motion due to clearance in the rotational joint. This issue can be addressed in the future using a magnetic latch that holds the gripper rigidly in place until impact.

IV. GRASPING DRONE SYSTEMS CONTROLLER

The goal of the grasping drone is to hit the target with the gripper at a specified velocity to successfully grasp it. The control scheme comprises three key elements: the onboard controller, a trajectory module, and a PID controller.

The onboard controller is used to command motor rates to maintain the desired velocity. Physically, this consists of an autopilot board, a companion computer, and motor controllers. The trajectory module computes a straight-line trajectory between the starting position, the goal position, and the end position. To maintain a constant pitch throughout the flight, the module is designed so that there is a constant velocity buffer before and after the goal position. The PID controller module commands the grasping drone to follow the desired trajectory. The controller takes in the position of the drone and the desired position to compute the desired velocity for the PX4 autopilot to track. The PX4's low-level controllers compute the required rotor rates to fly at the commanded velocity.

The control loop is depicted in Fig. 5. The trajectory module (orange) sends the desired position to the PID controller module, which then compares this value to the position determined by the mo-cap system (purple). These flight data (pink) then are sent between the modules. With this control scheme, precise control of the velocity of the drone at the time of impact with the target drone is achieved.

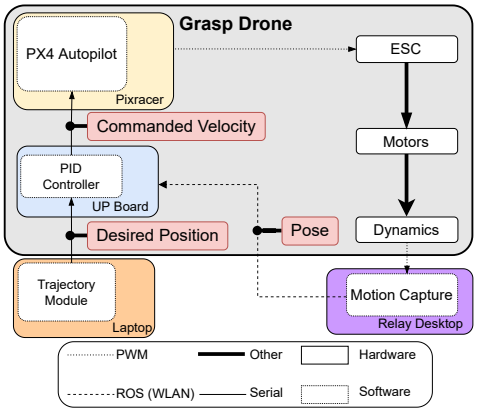

Fig. 5. The control scheme used to command the velocity and position of the drone for grasping. Modules in the shaded gray region run on the UP board physically on the drone. The orange region is the ground station.

V. EXPERIMENT AND VALIDATION

In this section, we present characterization experiments that were conducted to construct a sufficiency region in velocity space, which can be used in most commercially available flight controllers for aerial grasping. Flight experiments were subsequently conducted in a room equipped with mo-cap system to demonstrate the system capability.

A. Interaction Force Testing

The first step is to establish the forces needed to trigger the grasp sequence. The gripper is mounted on a 6-axis force and torque sensor (ATI Gamma), as shown in Fig. 6 left. Then, a random force is applied to the center of the gripper. The location of the contact can be determined based on the results of the force and moment readings. This wrench vector is then translated from the center of the force and torque sensor to the center of the gripper jaw. Empirically, with many trials, a limit surface can be plotted in force space (Fig. 6). This is the force sufficiency region: a surface in (x, y, z) force space that corresponds to the minimum force combinations required to trigger grasping. Any vector below this surface in the z direction will not trigger a grasp.

B. Launch Rail Setup and Data

To establish a connection between force and velocity, and to provide a repeatable testing platform for gripper design iteration, a pneumatic launch rail was constructed, as shown in Fig. 7. The grasping drone is mounted on a carriage on a linear rail. A piston is placed directly behind the carriage and is controlled by a solenoid attached to a pressure reservoir. The exit velocity at which the drone is launched is varied by adjusting the pressure in the reservoir. The linear rail ends shortly after the full stroke length of the piston. Then the drone, while still attached to the carriage, is launched and becomes ballistic. An electromagnet is placed $20\,\mathrm{cm}$ away from the end of the linear rail, and a smaller target drone is attached to this electromagnet. A relay switch is used to control the state of this electromagnet and can drop the target drone at any precise moment. The timing is such

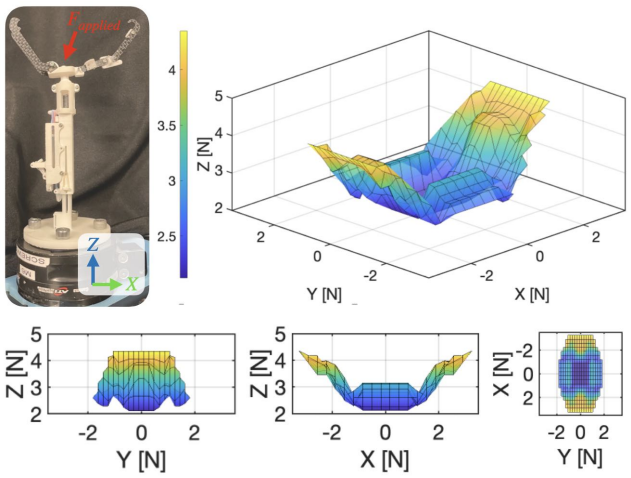

Fig. 6. Left: gripper mounted onto an ATI Gamma for force-space testing. A random force is applied to trigger the closing of the gripper. Right: limit surface constructed through data collected with the ATI testing setup.

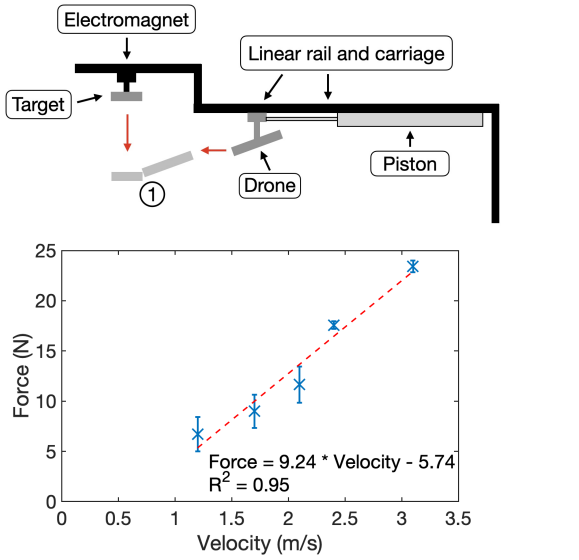

Fig. 7. Top: illustration of linear rail setup. The grasping drone is mounted on a linear rail. A piston accelerates the carriage drone to the desired exit velocity. A target drone is released through the control of an electromagnet. The timing is set such that the drone and target collide at point (1) while both are in ballistic motion. Bottom: the relationship between relative velocity and the measured peak impulse force at collision. The range of flight data collected at each velocity is marked with error bars with an average. A linear fit relates the velocity and peak impact force.

that the grasping drone and the target collide in mid-air, where the gripper catches the target drone. A structure of the same dimensions as the actual gripper is mounted on the grasping drone, with a very small and lightweight capacitive six-axis force-torque sensor mounted at its tip to measure the impact force [33]. The peak impact force is calculated from the recorded data. The entire experiment is recorded on a camera at 240 fps, with a timer in the frame. The velocities at impact can be calculated as a result. This experimental setup determines a relationship between peak impact force and relative velocity. As shown in Fig. 7, the relationship is approximately linear, providing a simple mapping between force space and velocity space for the system.

C. Force and Velocity Sufficiency Regions

Combining the aforementioned modeling and experimental setup, we can construct a sufficiency region for the gripper in force and then in velocity space. This sufficiency region is drone and gripper-specific. The following calculations are performed considering the drone used in the experiments, detailed in Sec. V-D.

First, a sufficiency region is constructed in force space. The lower bound of this sufficiency region is set by the minimal force needed to trigger, using data from the gripper acquired as described in Sec. V-A. The angles of this lower region are set by the rotational compliance in the mechanism, in this case $\beta_1 = 15°$ in the xy-plane and $\beta_2 = 30°$ in the xz-plane.

The upper-bound of this region is constrained by the maximum angular momentum that can be imparted to the capturing drone, consistent with the controller's limitations:

$$\Delta(I\boldsymbol{\omega}) = \int_{t_o}^{t_i} \boldsymbol{\tau_c} dt = \int_{t_o}^{t_g} \boldsymbol{\tau_u} dt \tag{9}$$

where $t_i - t_o = 0.025\,\mathrm{s}$ defines the duration of the impact force, which is recorded with the force and torque sensor during linear rail testing, and $t_g - t_0 = 0.1\,\mathrm{s}$ defines the duration of the grasping sequence. We note that $t_i < t_g$; the drone experiences a disturbance and has time to recover.

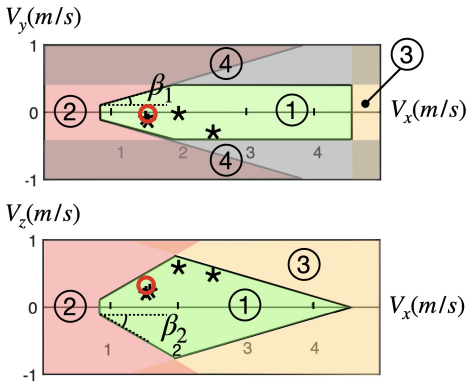

Fig. 8. Computed sufficiency region ① encloses the range of relative velocities at initial contact for which a catch should be possible. Region ② does not meet the minimum required triggering force. The sides are bounded by the maximum rotational compliance for the yaw direction and pitch direction; we denote the limits by β_1 and β_2 respectively. The upper bound is constrained by the maximum controllable impact force in the pitch direction ③ and the maximum allowable force in the yaw direction of the drone ④. Bold asterisks denote successful capture tests for a hovering target; red circles denotes capture of a moving target.

Although the controller used on the drone is globally stable [34] – meaning that given enough space, in a calm environment, and ignoring actuator limits, the drone will always be able to recover from an external wrench applied to it – the grasp sequence duration $t_g - t_o$ is chosen such that the drone will not hit the ground during recovery.

Taking eq. (1, 2), and the maximum drone thrust and torque from eq. (4), we can compute the maximum $\boldsymbol{\tau_c}$ and $\boldsymbol{f_e}$ that the drone can correct for in the given time interval. At the lower bound, with the force sufficiency

region experimentally determined in Sec. V-B we can also compute the corresponding minimum relative velocity needed for triggering, using the approximately linear mapping from force to torque as plotted in Fig. 7. The end result is a velocity sufficiency region, as plotted in Fig. 8 region ①. Velocity vectors in region ② fail due to inadequate force to trigger the gripper. Region ③ and region ④ are failures caused by excess $\boldsymbol{f_e}$ exceeding the control limit of the drone in the pitch and yaw direction, respectively. Note that they are overlapping regions where multiple failure cases occur. The values used in this calculation are listed in Table.V-C.

Parameter	Value
Max Motor Thrust	$3.16\,\mathrm{N}$
t_o	$0\,\mathrm{s}$
t_i	$0.025\,\mathrm{s}$
t_g	$0.1\,\mathrm{s}$
d	$\begin{bmatrix}0.1 & 0 & .03\end{bmatrix}\,\mathrm{m}$
L_x	$43\,\mathrm{mm}$
L_y	$62\,\mathrm{mm}$
Drone Mass	$550\,\mathrm{g}$
k_f	$1.83 \times 10^{-7}\,\mathrm{N\,s^2\,rad^{-2}}$
k_m	$2.83 \times 10^{-9}\,\mathrm{N\,m\,s^2\,rad^{-2}}$

TABLE I
PARAMETERS FOR GENERATING THE SUFFICIENCY REGION

D. Flight Demonstration

To demonstrate the function of the drone and gripper system, flight tests were performed in a room equipped with a motion capture (mo-cap) system (Fig. 9).

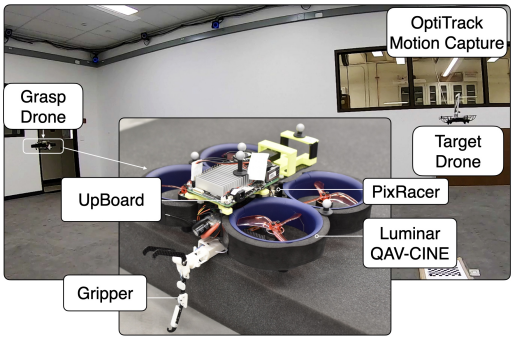

Fig. 9. Foreground: Photo of the gripper on the flight test platform. The grasping drone is a Lumenier QAV-CINE 3" frame with an mRo PixRacer R14 autopilot and an Intel UP Board companion computer. Background: Stanford's Boeing Flight and Autonomy Laboratory.

We employed a modified Parrot Mambo Fly drone (mass $85\,\mathrm{g}$) as the target based on the dynamic capability of the main grasping drone. The drone is set to hover at about $1\,\mathrm{m}$, and the grasping drone flight trajectory matches the altitude of the target. Inertial, position and visual data were recorded.

A trajectory, as shown in an example in Fig. 10, is planned, connecting the start, end, and goal positions with straight-line segments at a constant velocity. The desired velocity is kept constant throughout the grasping phase. This minimizes the angular movement of the gripper while flying. Each flight begins with both drones hovering at their starting position and ends after the grasping drone reaches the destination. The plot demonstrates that the drone is able to recover and keep flying after a typical aerial grasping event.

For initial flight tests, the gripper was rigidly attached to the drone, eliminating the swinging mechanism in Sec. III-A7, and a simple straight-line trajectory was chosen (i.e. no pitching forward to accelerate and level the drone to reduce the impact pitch angle right before impact). Therefore the pitch angle is coupled with the velocity of the grasp drone at impact. These effects reduce the maximum permitted relative velocity below the $4.5\,\mathrm{m\,s^{-1}}$ indicated in Fig. 8. Flight velocities were chosen such that the drone remains within a reduced sufficiency region, between 1.5 and $2.7\,\mathrm{m\,s^{-1}}$. Additional limiting factors included (i) the accuracy of the onboard controller following a set trajectory, (ii) the lack of tracking of the grasping target, and (iii) the lack of physical space with motion capture that would be needed for higher speeds and accelerations. Despite these limitations, the flight experiments confirmed the ability of an off-the-shelf autopilot to maintain control of the drone during and after collision using the gripper and suspension designed in Sec. III.

For aerial grasping and collision, the most important factor is the relative velocity between the grasping drone and the target. This velocity determines the interaction forces and dictates the speed required for grasping and the control required to recover after contact and acquisition. To demonstrate capturing a moving drone we conducted tests with the grasping drone flying at $2\,\mathrm{m\,s^{-1}}$ and the target at $0.5\,\mathrm{m\,s^{-1}}$. Due to a lack of target tracking, these tests were often not successful. However, as long as initial contact was made between the gripper and the target, the success rate was the same as for a hovering target. A typical result is shown with a red circle in Fig. 8. A composite photo of the chase and intercept sequence is shown in Fig. 1.

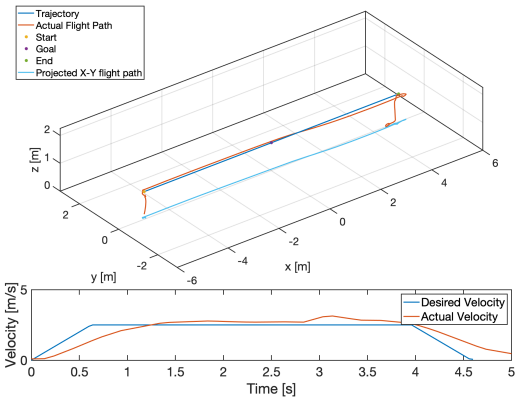

Fig. 10. An example test flight. The trajectory of the drone is shown in the top panel. The bottom plot shows the desired and actual velocity of the grasping drone. The bump after the collision (at $3\,\mathrm{s}$) is a result of the controller trying to catch up to the trajectory. Relative velocity at impact is plotted with an asterisk in Fig. 8 for reference.

VI. Conclusion and Future Work

We present an initial exploration of aerial grasp and capture of an airborne drone target. We introduced the concept of a sufficiency region for aerial grasping in velocity space and,

consistent with the corresponding design requirements, developed a fast, lightweight passive gripper that has the capability of performing aerial grasping. As drones are controlled with position and velocity commands as input, a grasp sufficiency region in velocity space is valuable for planning a collision – contrary to most drone control where collision avoidance is of utmost importance. For grippers intended to be used for aerial grasping by a drone, a passive mechanism has the advantage of being lightweight and, more importantly, fast-acting. Because of the nature of aerial grasping, the exact point of collision is unknown. With a passive mechanism, the grasp sequence is triggered mechanically, which minimizes the response time by not requiring a sense and compute control loop. This approach can increase the maximum relative velocity for aerial grasping maneuvers. The specific gripper mechanism presented in this work weighs only 4% of the body mass of the drone ($22.7\,\mathrm{g}$) and can close within $12\,\mathrm{ms}$ without knowing the exact timing of the collision between the object and the gripper.

As this is an initial exploration of aerial grasping, many areas warrant further investigation. First, implementing vision tracking of the target to the grasping drone would enable a full-fledged aerial pursuit and capture. This would also help the drone perform this maneuver in a real-world environment, without the aid of a motion capture system. Second, the swinging mechanism described in Sec. III-A7 can be further developed and tested to enable a higher relative velocity. Another approach to increase this upper bound is to decouple the pitch angle and gripper mechanism by implementing an actively controlled joint at the base of the gripper, or the inclusion of more sophisticated flight maneuvers. Lastly, the dynamic modeling can be expanded, instead of the simplified model used in this paper. This would produce a more accurate sufficiency region for a given system.

REFERENCES

[1] D. Floreano and R. J. Wood, "Science, technology and the future of small autonomous drones," *nature*, vol. 521, no. 7553, pp. 460–466, 2015.

[2] W. Roderick, M. Cutkosky, and D. Lentink, "Bird-inspired dynamic grasping and perching in arboreal environments," *Science Robotics*, vol. 6, no. 61, p. eabj7562, 2021.

[3] U. A. Fiaz, M. Abdelkader, and J. S. Shamma, "An intelligent gripper design for autonomous aerial transport with passive magnetic grasping and dual-impulsive release," in *2018 IEEE/ASME AIM*. IEEE, 2018, pp. 1027–1032.

[4] U. A. Fiaz, N. Toumi, and J. S. Shamma, "Passive aerial grasping of ferrous objects," *IFAC*, vol. 50, no. 1, pp. 10 299–10 304, 2017.

[5] C. C. Kessens, J. Thomas, J. P. Desai, and V. Kumar, "Versatile aerial grasping using self-sealing suction," in *2016 IEEE ICRA*. IEEE, 2016, pp. 3249–3254.

[6] M. A. Estrada, S. Mintchev, D. L. Christensen, M. R. Cutkosky, and D. Floreano, "Forceful manipulation with micro air vehicles," *Science Robotics*, vol. 3, no. 23, p. eaau6903, 2018.

[7] L. Hingston, J. Mace, J. Buzzatto, and M. Liarokapis, "Reconfigurable, adaptive, lightweight grasping mechanisms for aerial robotic platforms," in *2020 IEEE SSRR*. IEEE, 2020, pp. 169–175.

[8] A. McLaren, Z. Fitzgerald, G. Gao, and M. Liarokapis, "A passive closing, tendon driven, adaptive robot hand for ultra-fast, aerial grasping and perching," in *2019 IEEE/RSJ IROS*. IEEE, 2019, pp. 5602–5607.

[9] W. Stewart, E. Ajanic, M. Muller, and D. Floreano, "How to Swoop and Grasp Like a Bird With a Passive Claw for a High-Speed Grasping," *IEEE/ASME TMECH*, pp. 1–9, 2022.

[10] D. Mellinger, Q. Lindsey, M. Shomin, and V. Kumar, "Design, modeling, estimation and control for aerial grasping and manipulation," in *2011 IEEE/RSJ IROS*. IEEE, 2011, pp. 2668–2673.

[11] R. Spica, A. Franchi, G. Oriolo, H. H. Bülthoff, and P. R. Giordano, "Aerial grasping of a moving target with a quadrotor uav," in *2012 IEEE/RSJ IROS*. IEEE, 2012, pp. 4985–4992.

[12] J. Fishman, S. Ubellacker, N. Hughes, and L. Carlone, "Dynamic grasping with a" soft" drone: From theory to practice," in *2021 IEEE/RSJ IROS*. IEEE, 2021, pp. 4214–4221.

[13] J. Thomas, J. Polin, K. Sreenath, and V. Kumar, "Avian-inspired grasping for quadrotor micro uavs," in *International Design Engineering Technical Conferences and Computers and Information in Engineering Conference*, vol. 55935. ASME, 2013, p. V06AT07A014.

[14] J. Thomas, G. Loianno, K. Sreenath, and V. Kumar, "Toward image based visual servoing for aerial grasping and perching," *Proceedings - IEEE ICRA*, pp. 2113–2118, 2014.

[15] A. Rodriguez-Ramos, A. A.-F. H. Bavle, J. Rodriguez-Vazquez, L. L. M. Fernandez-Cortizas, R. A. S. Fernandez, A. Rodelgo, C. Santos, M. Molina, L. Merino, F. Caballero, and P. Campoy, "Autonomous Aerial Robot for High-Speed Search and Intercept Applications," 2021. [Online]. Available: http://arxiv.org/abs/2112.05465

[16] P. E. Pounds, D. R. Bersak, and A. M. Dollar, "Grasping from the air: Hovering capture and load stability," *Proceedings - IEEE ICRA*, pp. 2491–2498, 2011.

[17] R. Cory and R. Tedrake, "Experiments in fixed-wing uav perching," in *AIAA Guidance, Navigation and Control Conference and Exhibit*, 2008, p. 7256.

[18] M. T. Pope and M. R. Cutkosky, "Thrust-assisted perching and climbing for a bioinspired uav," in *Conference on Biomimetic and Biohybrid Systems*. Springer, 2016, pp. 288–296.

[19] A. L. Desbiens, A. T. Asbeck, and M. R. Cutkosky, "Landing , perching and taking off from," vol. 30, no. 3, pp. 355–370, 2011.

[20] C. E. Doyle, J. J. Bird, T. A. Isom, J. C. Kallman, D. F. Bareiss, D. J. Dunlop, R. J. King, J. J. Abbott, and M. A. Minor, "An avian-inspired passive mechanism for quadrotor perching," *IEEE/ASME TMECH*, vol. 18, no. 2, pp. 506–517, 2013.

[21] J. Thomas, M. Pope, G. Loianno, E. W. Hawkes, M. A. Estrada, H. Jiang, M. R. Cutkosky, and V. Kumar, "Aggressive flight with quadrotors for perching on inclined surfaces," *JMR*, vol. 8, no. 5, p. 051007, 2016.

[22] B. Bäuml, T. Wimböck, and G. Hirzinger, "Kinematically optimal catching a flying ball with a hand-arm-system," in *2010 IEEE/RSJ IROS*. IEEE, 2010, pp. 2592–2599.

[23] A. Namiki, Y. Imai, M. Ishikawa, and M. Kaneko, "Development of a high-speed multifingered hand system and its application to catching," in *Proceedings 2003 IROS (Cat. No. 03CH37453)*, vol. 3. IEEE, 2003, pp. 2666–2671.

[24] T. Lee, M. Leok, and N. H. McClamroch, "Geometric tracking control of a quadrotor uav on se (3)," in *49th IEEE conference on decision and control (CDC)*. IEEE, 2010, pp. 5420–5425.

[25] H.-N. Nguyen and D. Lee, "Hybrid force/motion control and internal dynamics of quadrotors for tool operation," in *2013 IEEE/RSJ IROS*. IEEE, 2013, pp. 3458–3464.

[26] S. Jung, "A position-based force control approach to a quad-rotor system," in *2012 9th URAI*, 2012, pp. 373–377.

[27] M. Fumagalli, R. Naldi, A. Macchelli, R. Carloni, S. Stramigioli, and L. Marconi, "Modeling and control of a flying robot for contact inspection," in *2012 IEEE/RSJ IROS*, 2012, pp. 3532–3537.

[28] S. Montambault and C. m. M. Gosselin, "Analysis of underactuated mechanical grippers," *J. Mech. Des.*, vol. 123, no. 3, pp. 367–374, 2001.

[29] G. A. Kragten and J. L. Herder, "The ability of underactuated hands to grasp and hold objects," *Mechanism and Machine Theory*, vol. 45, no. 3, pp. 408–425, 2010.

[30] H. Zhang, E. Lerner, B. Cheng, and J. Zhao, "Compliant bistable grippers enable passive perching for micro aerial vehicles," *IEEE/ASME TMECH*, vol. 26, no. 5, pp. 2316–2326, 2020.

[31] R. R. Ma and A. M. Dollar, "Linkage-based analysis and optimization of an underactuated planar manipulator for in-hand manipulation," *ASME JMR*, vol. 6, no. 1, p. 011002, 2014.

[32] N. J. Venable, *Birds of prey*. West Virginia University, Extension Service, 1996.

[33] X. A. Wu, S. A. Suresh, H. Jiang, J. V. Ulmen, E. W. Hawkes, D. L. Christensen, and M. R. Cutkosky, "Tactile sensing for gecko-inspired adhesion," in *2015 IEEE/RSJ IROS*. IEEE, 2015, pp. 1501–1507.

[34] D. Brescianini, M. Hehn, and R. D'Andrea, "Nonlinear quadrocopter attitude control: Technical report," ETH Zurich, Tech. Rep., 2013.